# Journal Pre-proof


A model for the bio-mechanical stimulus in bone remodelling as a diffusive signalling agent for bones reconstructed with bio-resorbable grafts

R. Allena, D. Scerrato, A.M. Bersani, I. Giorgio

PII: S0093-6413(23)00052-6
DOI: https://doi.org/10.1016/j.mechrescom.2023.104094
Reference: MRC 104094

To appear in: *Mechanics Research Communications*

Received date : 9 September 2022
Revised date : 27 January 2023
Accepted date : 14 March 2023

Please cite this article as: R. Allena, D. Scerrato, A.M. Bersani et al., A model for the bio-mechanical stimulus in bone remodelling as a diffusive signalling agent for bones reconstructed with bio-resorbable grafts, *Mechanics Research Communications* (2023), doi: https://doi.org/10.1016/j.mechrescom.2023.104094.

# A model for the bio-mechanical stimulus in bone remodelling as a diffusive signalling agent for bones reconstructed with bio-resorbable grafts

R. Allena[a], D. Scerrato[b,c], A. M. Bersani[b,c,d], I. Giorgio[b,d,e]

[a] *Université Côte d'Azur, Laboratoire Jean Alexandre Dieudonné UMR CNRS 7351, Nice, France,*
[b] *International Research Center for the Mathematics and Mechanics of Complex Systems (M&MoCS), University of L'Aquila,*
[c] *Dipartimento di Ingegneria Meccanica e Aerospaziale (DIMA), University of Rome La Sapienza,*
[d] *Gruppo Nazionale per la Fisica Matematica (GNFM) of the Istituto Nazionale di Alta Matematica (INdAM, Italy),*
[e] *Dipartimento di Ingegneria Civile, Edile-Architettura e Ambientale (DICEAA), University of L'Aquila,*

**Abstract**

Bone remodelling is a self-adaptive process occurring in bone living tissue to optimize its mechanical response to environmental demands. Some cells, namely osteocytes, monitor this response and communicate with other cells, osteoblasts, and osteoclasts, in charge of synthesizing or reabsorbing solid bone in order to acquire the mechanical strength required for bone functioning. In this paper, we employ a diffusive model of a mechanical stimulus to describe at the organ level the mechanisms involved in the transduction of the information and activation of the remodelling process. This stimulus is produced after a bone deformation, and thus we assume it depends on strain energy density. The system that we analyse is a bone sample with a resorbable graft. Mainly, we focus on the interaction between the two components of the system. From a mechanical point of view, we consider a mixture of two solid phases described by a poro-viscoelastic model. The results show a general behaviour that matches the expected outcomes and confirms the usefulness of the proposed model.

*Keywords:* Bone remodelling, bone-graft interaction, porous resorbable scaffold, Fick's laws of diffusion, bio-mechanical stimulus

## 1. Introduction

Bone is a biological tissue able to adapt itself to its environment. While conceiving a similar artificial material remains a challenge [1, 2], one can consider integrating a synthetic graft into the bone structure to obtain some effective clinical results. In this context, the main objective is to optimize the mechanical and geometrical properties of the graft in order to promote bone healing and remodelling. Our primary focus here is, then, to analyse the interaction between the graft and the bone with a computationally efficient and reliable model. A few elements must be considered. First, the graft must be porous and sufficiently tough to support the external mechanical loads. Second, the stimulus [3, 4, 5] that activates the adaptation process has a crucial role in the remodelling phenomenon. In fact, it can be considered as a macroscopic source of canalicular flow, representing the mechanical state of the tissue, and may influence the cellular behaviour over time [6, 7, 8]. Third, we assume that both graft and bone micro-structures are very similar and can therefore be described within the same formulation but with different mechanical properties. Finally, in our previous work [9], a second gradient theory was employed to capture the effects of the bone micro-structure due to its multi-scale organization and heterogeneity [10, 11, 12, 13, 14, 15]. Such a theory is consistent when considering long trabeculae whose mechanical response may have macroscopic consequences. Here, we have made the hypothesis that the trabeculae are rather short and stocky, thus, a first gradient theory is sufficient to describe their behaviour [16, 17]. Additionally, we want to simplify our mechanical approach to focus more on the mechano-biological aspect of the problem, i.e., the mechanical stimulus.

The rationale of the paper is to examine the simplified case of isotropic bone tissue in the presence of a graft as a preliminary step to move forward with the more realistic case of anisotropic or orthotropic tissue as further development. The central aspect we investigate herein is the effects of the stimulus treated as a signal that can diffuse in the bone and possibly in an artificial porous graft employed as a scaffold for the synthesis of new bone. For anisotropic or orthotropic tissues, we have to deal with the evolution of many material parameters; however, for each of them, we can imagine using the same transmission paths of stimulus signalling that we have examined in the present work.

## 2. The model

### *2.1. Mechanical formulation*

For the present study, we employ the same system as the one analysed in [9], consisting of trabecular bone tissue surrounding an artificial graft. The aim of the graft is to promote the healing process by ensuring a mechanical junction between the broken bone and a scaffold, which facilitates the remodelling process. Both the bone and the graft are considered porous materials. The former shows different kinds of porosity, such as lacunar-canalicular, inter-trabecular, or collagen-apatites porosity [18]. The latter is constituted by interconnected inner cavities that make cells' functions (i.e., migration and colonization) possible as well as the supply of nutrients.

The displacement $\mathbf{u}$ and the current Lagrangian porosity $\phi$ are defined as

$$\mathbf{u} = \mathbf{x} - \mathbf{X}$$
$$\phi(\mathbf{X}, t) = n[\chi(\mathbf{X}, t)]J(\mathbf{X}, t)$$

where $\mathbf{X}$ is any particle of the system in the reference configuration, $\mathbf{x} = \chi(\mathbf{X}, t)$ is the position of the particle $\mathbf{X}$ in the current configuration, $n[\chi(\mathbf{X}, t)]$ is the Eulerian porosity and $J = \det(\mathbf{F}) = \det(\nabla\chi(\mathbf{X}, t))$ [19].

During the evolution, the stiffness of the bone/graft system may assume much softer values than the initial ones, and consequently, the deformed configuration can be different from the reference one. To be consistent, we introduce a nonlinear behaviour in the simplest possible way, as follows, assuming that we remain in the elastic response of the considered system. Moreover, the reason for such a choice lies also in the complexity of bone microstructure, i.e., the trabeculae, that sometimes involves non-linear behaviours notwithstanding small strain regime as, for instance, documented in [20]. We refrain here from considering material nonlinearities because we want to focus our attention on the stimulus model rather than the mechanical behaviour.

Thus, the finite strain tensor $\mathbf{E}_{ij}(\mathbf{X}, t)$ and the change of the Lagrangian porosity $\zeta(\mathbf{X}, t)$ read

$$\mathbf{E}_{ij}(\mathbf{X}, t) = \frac{1}{2}(u_{i,j} + u_{j,i} + u_{i,k}u_{k,j})$$
$$\zeta(\mathbf{X}, t) = \phi(\mathbf{X}, t) - \phi^*(\mathbf{X}, t)$$

with $\phi(\mathbf{X}, t)$ and $\phi^*(\mathbf{X}, t)$ the Lagrangian porosities at the current and reference configurations, respectively.

The system is constituted of two parts, the bone and the bio-resorbable graft, but it can be studied as a whole by using the mixture theory. More specifically, the bone shows a solid phase and a porous space typically filled with bone marrow, interstitial fluids, blood, bone cells, etc. The graft is porous, too, and its pores are filled with organic matter as soon as it is implanted [4, 21, 22]. Although the initial conditions for the two parts are very similar, they evolve rather differently throughout time. In fact, during the remodelling process, in the graft, they may coexist three phases: bio-resorbable material, bone, and physiological fluid.

According to the mixture theory, $\phi^*(\mathbf{X}, t)$ can be written as

$$\phi^*(\mathbf{X}, t) = 1 - \left(\frac{\rho_b^*(\mathbf{X}, t)}{\hat{\rho}_b} + \frac{\rho_g^*(\mathbf{X}, t)}{\hat{\rho}_g}\right) \tag{1}$$

where $\frac{\rho_b^*(\mathbf{X},t)}{\hat{\rho}_b}$ and $\frac{\rho_g^*(\mathbf{X},t)}{\hat{\rho}_g}$ are the volume fractions of the constituents and $\rho_b^*$ and $\rho_g^*$ are the apparent mass densities of bone tissue and graft artificial material in the reference configuration, respectively. The superimposed hat denotes the mass densities evaluated considering the precise volume occupied by those phases. Since the apparent mass densities of different phases depend on environment mechanical excitations and time, we assume that the reference configuration is linked to the apparent mass density in the reference state, i.e., when zero stress occurs. The current porosity $\phi$ can be expressed as

$$\phi = \phi^* + \zeta \tag{2}$$

The energy density can be expressed as [23, 24]

$$\begin{aligned}\mathscr{E} = U_s + U_f + U_{fg} + U_{fm} = \\ \underbrace{\frac{1}{2}\lambda(\rho_b^*, \rho_g^*)E_{ii}E_{jj} + \mu(\rho_b^*, \rho_g^*)E_{ij}E_{jj}}_{U_s} + \\ \underbrace{\frac{1}{2}K_1(\rho_b^*, \rho_g^*)\zeta^2}_{U_f} + \underbrace{\frac{1}{2}K_2\zeta_{,i}\zeta_{,i}}_{U_{fg}} - \underbrace{K_3(\rho_b^*, \rho_g^*)\zeta E_{ii}}_{U_{fm}}\end{aligned} \tag{3}$$

where all the material parameters are considered as a function of the apparent mass density of the bone and the graft evaluated in the reference configuration. The subscripts stand for solid part (s), fluid one (f), a contribution related to the gradient of porosity (fg), and a fluid-solid coupling (fm), in the given order. Such an expression is the simplest when considering bone and graft as isotropic materials.

The Lamé coefficients $\lambda$ and $\mu$ can be written as

$$\lambda = \frac{\nu Y(\rho_b^*, \rho_g^*)}{(1+\nu)(1-2\nu)}, \qquad \mu = \frac{Y(\rho_b^*, \rho_g^*)}{2(1+\nu)} \tag{4}$$

with

$$Y = Y_b^{max}\left(\frac{\rho_b^*}{\hat{\rho}_b}\right)^2 + Y_g^{max}\left(\frac{\rho_g^*}{\hat{\rho}_g}\right)^2 \tag{5}$$

The three parameters $K_1, K_2$, and $K_3$ allow taking into account the presence of the pores and their effects on the macroscopic deformation of the system under study. $K_1$ is a compressibility coefficient defined in [9] as the volume of fluid released from unit bulk volume per unit decrease in pore pressure under the condition of constant confining stresses [23]. $K_2$ is the aptitude of the system to oppose the establishment of a gradient of porosity, and it is assumed to be constant [9]. Finally, $K_3$ couples the micro-structure due to pores and the bulk solid [9, 23]. Some procedures for the evaluation of material parameters in complex systems can be found in [25, 26, 27, 28, 29]. The expressions of $K_1, K_2$ and $K_3$ can be found in [9]. As mentioned in [9], several sources of dissipation may appear in the system at the interface between bone and graft, in the fluid that fills the pores, in the bone solid matrix, or at the interface between the solid and the fluid phase for instance. We have decided to consider all these sources from a macroscopic point of view using a Rayleigh functional that can be explicitly written as

$$2\,\mathscr{D}_s = 2\,\mu^v\left(\dot{E}_{ij}\dot{E}_{ij} - \frac{1}{3}\dot{E}_{ii}\dot{E}_{jj}\right) + k^v\dot{E}_{ii}\dot{E}_{jj} \tag{6}$$

employing a Kelvin—Voigt model, where $\dot{E}$ is the solid-matrix rate of deformation and $\mu^v$ and $k^v$ are two viscous coefficients.

In the system, at least two time scales should be considered. On the one hand, the one related to the applied mechanical loads like walking, which is in the order of a few seconds [30]. On the other hand, the one related to the remodeling process, which is in the order of a few months [31]. Here, we only take into account the latter.

We apply the Generalized Principle of Virtual Work as follows

$$\int_{\mathscr{B}^*}\delta\mathscr{E}\,d\mathscr{B}^* + \int_{\mathscr{B}^*}\frac{\partial\mathscr{D}_s}{\partial\dot{E}_{ij}}\delta E_{ij}\partial\mathscr{B}^* = \int_{\mathscr{B}^*}\delta\mathscr{W}^{ext}d\mathscr{B}^* \tag{7}$$

where $\delta\mathscr{W}^{ext}$ describes the virtual work done by external loads, which can be written as

$$\delta\mathscr{W}^{ext} = \int_{\partial_\tau\mathscr{B}^*}\tau_i\delta u_i d\mathscr{S}^* + \int_{\partial_\Xi\mathscr{B}^*}\Xi\delta\zeta d\mathscr{S}^* \tag{8}$$

where the first term takes into account the forces per unit surface (i.e. $\tau_i$ on the part of the boundary $\delta_\tau\mathscr{B}^*$) and the second term is related to the effects of a pore pressure $\Xi$ on the boundary $\delta_\Xi\mathscr{B}^*$.

The interactions between the bone tissue and the artificial bio-resorbable graft are taken into account via an extra contribution of the virtual work as it has been proposed in [9].

*2.2. Remodelling formulation*

In this section, we describe the bone remodelling process once the graft has been implanted. The evolution of the apparent mass density of both the bone ($\rho_b$) and the graft ($\rho_g$) is described in the reference configuration. More specifically, we express the time derivatives of the mass densities as a function of a mechanical stimulus $S(\mathbf{X}, t)$ and the porosity $\phi(\mathbf{X}, t)$ as follows [4]

$$\begin{cases} \dfrac{\partial \rho_b^*}{\partial t}(\mathbf{X}, t) = A_b(S)H(\phi) & \text{with} \quad 0 < \rho_b^* \leq \hat{\rho}_b \\ \dfrac{\partial \rho_g^*}{\partial t}(\mathbf{X}, t) = A_g(S)H(\phi) & \text{with} \quad 0 < \rho_g^* \leq \rho_g^*(\mathbf{X}, 0) \end{cases} \tag{9}$$

$A_b$ and $A_g$ being two functions assumed to be piece-wise linear as follows

$$A_{\{b,g\}}(S) = \begin{cases} s_{\{b\}}S & \text{for} \quad S \geq 0 \\ r_{\{b,g\}}S & \text{for} \quad S < 0 \end{cases} \tag{10}$$

where the coefficients $s$ and $r$ are the rates of growth and resorption, respectively and the symbol $b, g$ stands for the alternative between $b$, i.e., bone, and $g$, i.e., graft.

The function $H(\phi)$ accounts for the porosity that plays a critical role during the remodelling process. In fact, the pores allow the bone cells to reach the more remote zones of the system and operate to remove or synthesize bone tissue as demanded by the environmental external loads. Therefore, two scenarios can appear: either i) the porosity is low, there is no room for the bone cells and the densities do not change or ii) the porosity is high, the remodelling cannot take place. Therefore, we have assumed a maximal value of $H$ for the porosity of about 0.6, which provides the most efficient conditions for bone remodelling when porosity is far away from the two extreme cases. [32].

The mechanical stimulus $S$ is conventionally sensed by the osteocytes and consents bone to monitor and adapt its overall state. Here, we assume that both the osteoclasts and osteoblasts modify the solid phases and, consequently the mechanical properties (i.e. the stiffness) of the system. In the present work, the stimulus has been expressed through a diffusion equation as follows [32]

$$\frac{\partial S}{\partial t} - \kappa \Delta S + \beta S = f(r_b^*)(U_s + U_f + U_{fm}) \tag{11}$$

where $\kappa$ and $\beta$ are two scalars and the latter is activated only when $S > 0$. The function $f(r_b^*)$ is a proper signalling weight. The initial conditions for the stimulus are set to be equal to 0 in the graft and $4.275 \times 10^{-9}$ in the bone, corresponding to an equilibrium state, namely homeostasis. Regarding the boundary conditions, we set Neumann ones, assuming no stimulus flux is exchanged with the outside.

In our formulation, we remark that boundary conditions affect the mass density evolution only indirectly. The crucial contribution is due to the boundary conditions specifying the mechanical interaction with the external world and driving the bone functional adaptation. A secondary effect worth mentioning comes from the boundary conditions of the stimulus equation since the actual distribution of the stimulus, and then the "picture" of the mechanical state, depends on it.

## 3. Numerical implementation for an illustrative case

In this section, we detail the numerical implementation of our formulation for an illustrative two-dimensional (2D) case. As in [9], we consider a beam of length $L = 2$ cm and width $w = 0.5$ cm. The beam is constituted of three regions: two bone regions (B) and the central one representing the graft (G). The material sequence is then BGB. The left side of the beam is constrained to avoid longitudinal displacements but keeping free the transverse ones (see Fig. 1). On the right side, a force per unit line $f(X_2, t)$ with a symmetric linear distribution along the transverse direction is applied. The longitudinal component of the force can be written as

$$f(X_2, t) = \left(\frac{X_2}{w} - \frac{1}{2}\right)[F_0 + F_1 \sin(\Omega t)] \tag{12}$$

where $F_0 = \psi Y_b^{max}$ and $F_1 = F_0/2$ are two nominal forces and $\Omega$ is the frequence. The model parameters are reported in Table 1.

The numerical simulations have been performed through a finite element analysis using COMSOL Multiphysics.

| | |
|---|---|
| $\hat{\rho}_b$ (kg/m$^3$) | 1800 |
| $\hat{\rho}_g$ (kg/m$^3$) | 1800 |
| $\nu$ | 0.3 |
| $Y_b^{max}$ (GPa) | 17 |
| $Y_g^{max}$ (GPa) | 13.6 |
| $\nu^v$ (N s/m$^2$) | 2.57x10$^{12}$ |
| $k^v$ (N s/m$^2$) | 2.06x10$^{12}$ |
| $s_b$ (s/m$^2$) | 1.27x10$^{-7}$ |
| $r_b$ (s/m$^2$) | 1.06x10$^{-7}$ |
| $r_g$ (s/m$^2$) | 1.59x10$^{-7}$ |
| $\kappa$ (m$^2$/s) | 1.6x10$^{-4}$ |
| $\beta$ | 0.6 |
| $\psi$ (N) | 1.68x10$^{-3}$ |
| $\Omega$ (Hz) | 8.27x10$^{-6}$ |

Table 1: Material parameters of the model used in the numerical simulations.

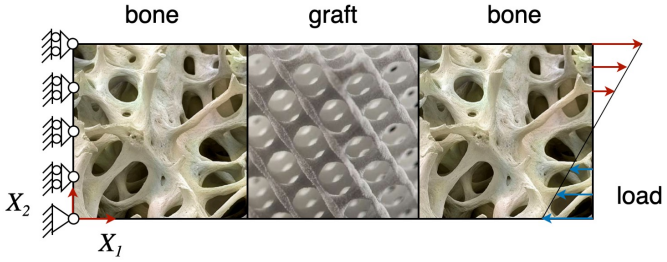


Figure 1: Schematic representation of the 2D system under study. The sample is constituted by two bone (B) regions and a graft (G) region in the middle in a BGB sequence.

## 4. Results and discussion

We have tested two sizes of the graft, specifically $L_g = 0.8$ cm and $L_g = 0.4$ cm, corresponding to 40% and 20% of the total length $L$ of the specimen. At the initial configuration, the volume fraction of the bone ($\frac{\rho_b^*}{\hat{\rho}_b}$) and the graft ($\frac{\rho_g^*}{\hat{\rho}_g}$) have been fixed to 0.5. To be consistent with a practical case and to be able to appreciate the effects of mechanical stimulation on the remodelling process, the analysed time period is equal to 15 weeks.

In Fig. 2, we show the volume fraction of bone (2a and b) and graft (2c and d) at the final configuration for the long (2a and c) and short (2b and d) graft, respectively. One can observe that for both long and short grafts, bone has been synthesized also in the central zone where the graft is implanted. The results depend on the initial distribution of the stimulus. In fact, at the beginning of the simulation, the stimulus is equal to zero in the graft (i.e. no osteocytes are present), whereas, at the end of the simulation, the stimulus has diffused inside the graft inducing the synthesis of bone in this region too. In this test, newly synthesised bone colonises the outer part of the sample preferentially, including the graft. On the contrary, the central part is characterized by losing graft mass without a relevant gaining of bone tissue. This evolution agrees with the natural distribution of bone density, which is typically denser in the outer part of bones and has high porosity in the inner regions. According to functional adaptation, the mass density increases where the strain is more elevated. Indeed, it is worth noting that the obtained mass density pattern matches the distribution of the strain energy that has been used here as a descriptor of the mechanical state of the bone system, as we hypothesised.

In Fig. 3, the distribution of the change of porosity $\zeta$ at the initial (3a and c) and at the final (3b and d) configurations for the long (3a and b) and short (3c and d) graft is reported. Fig. 3 shows that the deformation involving the porosity is localised in the vicinity of the outer regions, while no significant deformation is observed in the central zone, as expected. We can observe a low level of porosity deformation and the differences between the bone and the graft regions at the end of the simulation.

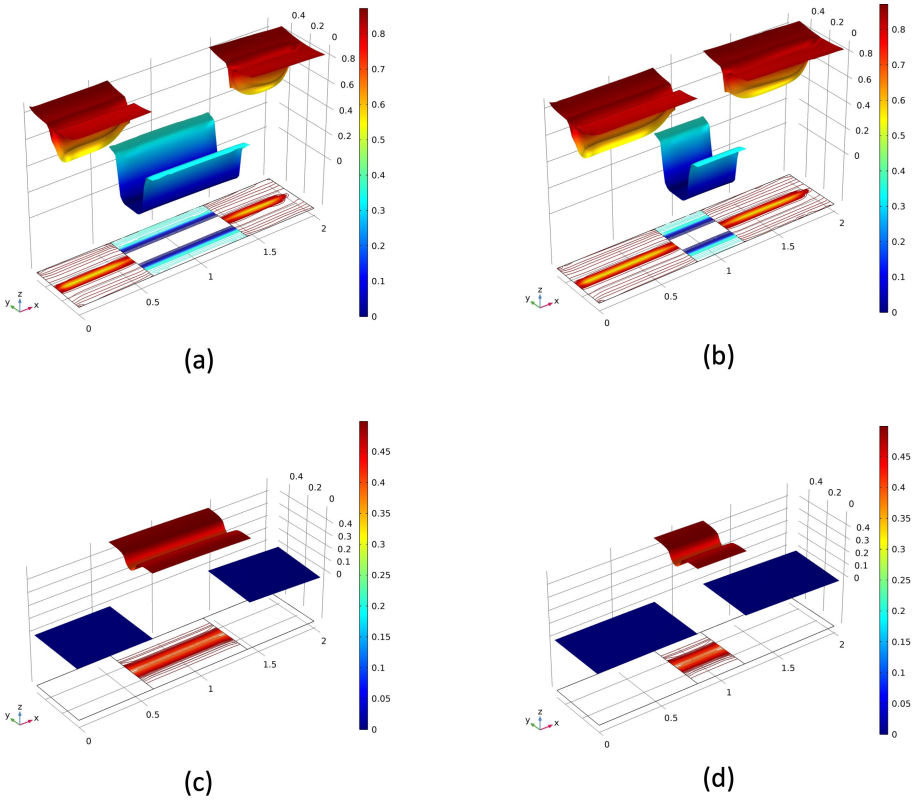


Figure 2: Plots of the volume fraction of bone $\frac{\rho_b^*}{\hat{\rho}_b}$ (a and b) and graft $\frac{\rho_g^*}{\hat{\rho}_g}$ (c and d) at the final configuration for $L_g = 0.8$ (a and c) and $L_g = 0.4$ (b and d).

The average stored energy decreases over time because the mass density of the system increases and, consequently, its overall stiffness, which leads to a lower strain (Fig. 4). As for the porosity $\zeta$, we also observe a clear difference between the bone and the graft since a different distribution of matter, namely the percentage of the phases, is present in the various regions.

Overall the results show that with a sufficiently high external load, the graft can be partially fulfilled by bone. Additionally, the final composition of the system (i.e. bone versus graft) depends also on the rates of bone synthesis and resorption of both phases. Finally, even though the formulation is different from the one presented in [9], we have obtained similar results for the synthesis/resorption of the bone/graft sample. In the previous work [9], the stimulus was directly evaluated by an explicit integral form. On the contrary, in the present work, we propose to apply the diffusion equation to assess the stimulus in a complex system made of bone and a resorbable artificial material. This approach is computationally more efficient since solving a PDE is more straightforward numerically than computing a convolution integral for each time step. From a physical perspective, considering the stimulus as a "vehicle" carrying the state information of the tissue and diffusing within it seems to be a rather educated guess. Naturally, there are some differences in the results of the two methods. For the direct integral formulation, setting the influence distance of osteocytes much smaller than the sample size allows us to see a more significant difference in the evolution of graft mass density for different sizes. Instead, in the present case, the diffusion character of the stimulus combined with the sink term of its metabolic resorption makes the differences in the mass evolution for different grafts less marked at the scale we examined. However, this is just preliminary work to understand if the proposed formulation is able to cover some typical behaviours that occur in the remodelling process. We believe this approach is promising and deserves further investigation because of the obtained results.

Finally, to corroborate the proposed continuum approach, we can consider that using a micro-computed tomography (micro-CT) analysis, it is possible to obtain a detailed picture of the micromorphology of tra-

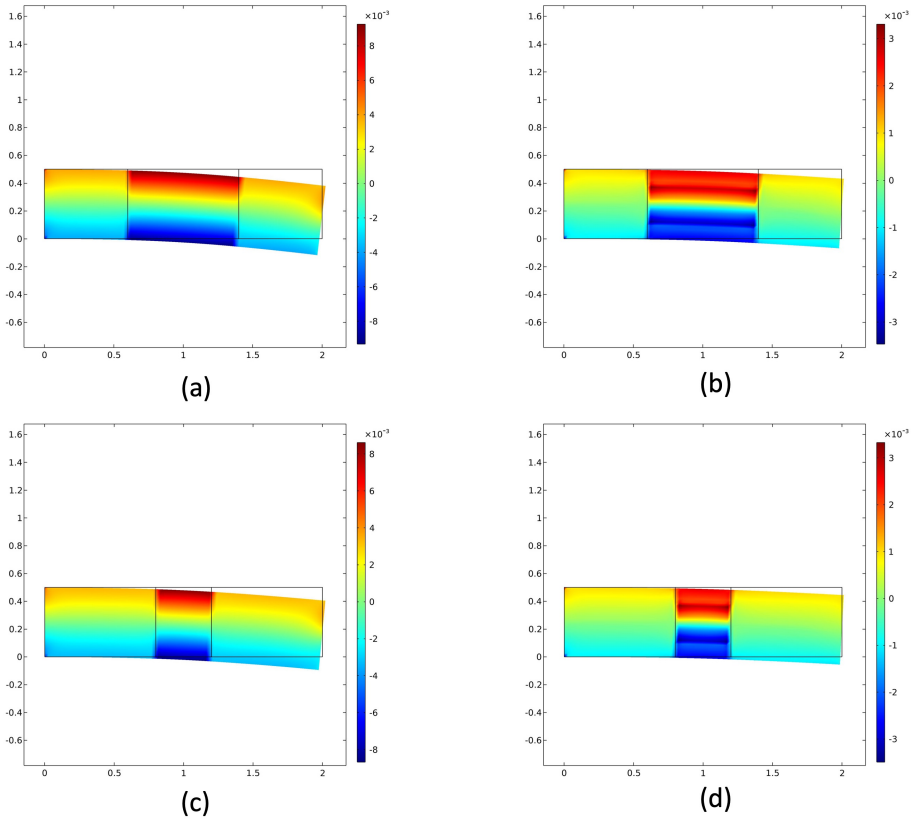


Figure 3: Distribution of the change of porosity $\zeta$ for $L_g = 0.8$ (a and c) and $L_g = 0.4$ (b and d) at the beginning (a and c) and at the end of the simulation (b and d).

becular bone tissue, including the presence of a bioresorbable graft, experimentally. With this information, the apparent mass density of the bone system can be obtained and, therefore, compared with the numerical simulations performed.

**Acknowledgement**

The authors want to express their deepest gratitude to Tomasz Lekszycki for the fruitful and stimulating discussions about the topic of the paper.

**References**

[1] S. H. Cho, H. M. Andersson, S. R. White, N. R. Sottos, P. V. Braun, Polydimethylsiloxane-based self-healing materials, Advanced Materials 18 (8) (2006) 997–1000.

[2] K. S. Toohey, N. R. Sottos, J. A. Lewis, J. S. Moore, S. R. White, Self-healing materials with microvascular networks, Nature materials 6 (8) (2007) 581–585.

[3] G. Beaupré, T. Orr, D. Carter, An approach for time-dependent bone modeling and remodeling–theoretical development, J. Orthop. Res. 8 (5) (1990) 651–661.

[4] T. Lekszycki, F. dell'Isola, A mixture model with evolving mass densities for describing synthesis and resorption phenomena in bones reconstructed with bio-resorbable materials, ZAMM - Z. Angew. Math. Mech 92 (6) (2012) 426–444.

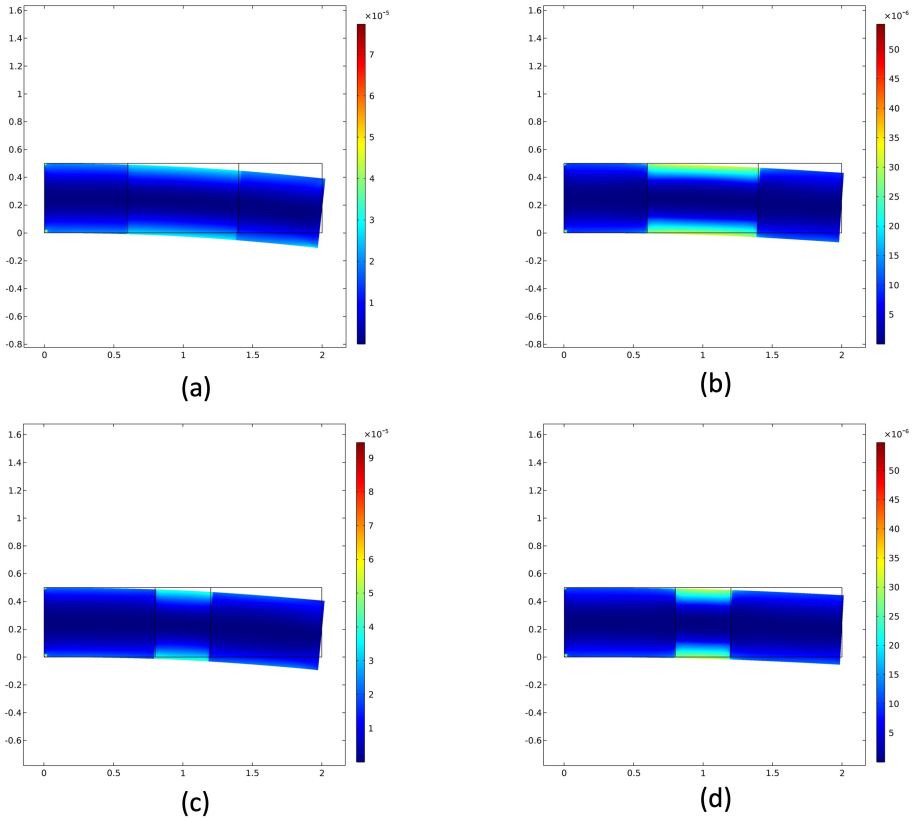


Figure 4: Distribution of the elastic energy density $U_s$ for $L_g = 0.8$ (a and c) and $L_g = 0.4$ (b and d) at the beginning (a and c) and at the end of the simulation (b and d).

[5] D. George, R. Allena, Y. Remond, A multiphysics stimulus for continuum mechanics bone remodeling, Math. Mech. Complex Syst. 6 (4) (2018) 307–319.

[6] N. Branecka, T. Lekszycki, Experimental methods of living cells mechanical loading, Contin. Mech. Thermodyn (2022) 1–19.

[7] D. George, R. Allena, C. Bourzac, S. Pallu, M. Bensidhoum, H. Portier, Y. Rémond, A new comprehensive approach for bone remodeling under medium and high mechanical load based on cellular activity, Math. Mech. Complex Syst. 8 (4) (2020) 287–306.

[8] A. M. Bersani, G. Dell'Acqua, Is there anything left to say on enzyme kinetic constants and quasi-steady state approximation?, J. Math. Chem. 50 (2) (2012) 335–344.

[9] D. Scerrato, A. M. Bersani, I. Giorgio, Bio-inspired design of a porous resorbable scaffold for bone reconstruction: A preliminary study, Biomimetics 6 (1) (2021).

[10] D. George, C. Spingarn, C. Dissaux, M. Nierenberger, R. A. Rahman, Y. Rémond, Examples of multiscale and multiphysics numerical modeling of biological tissues, Bio-Med. Mater. Eng. 28 (s1) (2017) S15–S27.

[11] I. Goda, M. Assidi, S. Belouettar, J. Ganghoffer, A micropolar anisotropic constitutive model of cancellous bone from discrete homogenization, J. Mech. Behav. Biomed. Mater. 16 (2012) 87–108.

[12] I. Goda, R. Rahouadj, J.-F. Ganghoffer, Size dependent static and dynamic behavior of trabecular bone based on micromechanical models of the trabecular architecture, Int. J. Eng. Sci. 72 (2013) 53–77.

[13] N. Branecka, M. E. Yildizdag, A. Ciallella, I. Giorgio, Bone remodeling process based on hydrostatic and deviatoric strain mechano-sensing, Biomimetics 7 (2) (2022) 59.

[14] A. Ciallella, Research perspective on multiphysics and multiscale materials: a paradigmatic case, Contin. Mech. Thermodyn 32 (3) (2020) 527–539.

[15] G. La Valle, A new deformation measure for the nonlinear micropolar continuum, ZAMP - Z. fur Angew. Math. Phys 73 (2) (2022) 1–26.

[16] C. Chesnais, C. Boutin, S. Hans, Wave propagation and non-local effects in periodic frame materials: Generalized continuum mechanics, Math. Mech. Solids. 20 (8) (2015) 929–958.

[17] G. Rosi, L. Placidi, N. Auffray, On the validity range of strain-gradient elasticity: a mixed static-dynamic identification procedure, Eur. J. Mech. A/Solids 69 (2018) 179–191.

[18] S. C. Cowin, Bone poroelasticity, J. Biomech. 32 (3) (1999) 217–238.

[19] O. Coussy, Poromechanics, John Wiley & Sons, 2004.

[20] E. F. Morgan, O. C. Yeh, W. C. Chang, T. M. Keaveny, Nonlinear behavior of trabecular bone at small strains, J. Biomech. Eng. 123 (1) (2001) 1–9.

[21] Y. Lu, T. Lekszycki, Modelling of bone fracture healing: influence of gap size and angiogenesis into bioresorbable bone substitute, Math. Mech. Solids. 22 (10) (2017) 1997–2010.

[22] E. Bednarczyk, T. Lekszycki, A novel mathematical model for growth of capillaries and nutrient supply with application to prediction of osteophyte onset, ZAMP - Z. fur Angew. Math. Phys 67 (4) (2016) 1–14.

[23] M. A. Biot, Mechanics of deformation and acoustic propagation in porous media, J. Appl. Phys. 33 (4) (1962) 1482–1498. doi:10.1063/1.1728759.

[24] S. C. Cowin, J. W. Nunziato, Linear elastic materials with voids, J. Elast. 13 (2) (1983) 125–147.

[25] B. E. Abali, C.-C. Wu, W. H. Müller, An energy-based method to determine material constants in nonlinear rheology with applications, Contin. Mech. Thermodyn 28 (5) (2016) 1221–1246.

[26] E. Barchiesi, A. Misra, L. Placidi, E. Turco, Granular micromechanics-based identification of isotropic strain gradient parameters for elastic geometrically nonlinear deformations, ZAMM-Z. fur Angew. Math. Mech 101 (11) (2021) e202100059.

[27] R. Fedele, Simultaneous assessment of mechanical properties and boundary conditions based on Digital Image Correlation, Exp. Mech. 55 (2015) 139–153.

[28] M. Valmalle, A. Vintache, B. Smaniotto, F. Gutmann, M. Spagnuolo, A. Ciallella, F. Hild, Local-global DVC analyses confirm theoretical predictions for deformation and damage onset in torsion of pantographic metamaterial, Mech. Mater (2022) 104379.

[29] M. Amar, D. Andreucci, P. Bisegna, R. Gianni, Homogenization limit for electrical conduction in biological tissues in the radio-frequency range, C.R. - Mec 331 (7) (2003) 503–508.

[30] P. Heinemann, M. Kasperski, Damping induced by walking and running, Procedia Eng. 199 (2017) 2826–2831.

[31] E. F. Eriksen, Cellular mechanisms of bone remodeling, Rev. Endocr. Metab. Disord. 11 (4) (2010) 219–227.

[32] I. Giorgio, F. dell'Isola, U. Andreaus, F. Alzahrani, T. Hayat, T. Lekszycki, On mechanically driven biological stimulus for bone remodeling as a diffusive phenomenon, Biomech. Model. Mechanobiol 18 (6) (2019) 1639–1663.

Manuscript number: MRC-D-22-00234

The authors declare that they have no conflict of interest.